Superlubricity controlled by the multiatomic nature of nanocontacts

Ali Sadeghi
Department of Physics, Shahid Beheshti University, G.C., Evin, 19839-63113 Tehran, Iran

(Received 8 April 2018; revised manuscript received 1 June 2018; published 8 August 2018)

Within the context of dry friction, the ultralow friction regime has been reported at various atomically small contacts. Realization of large superlubric contacts under ordinary environmental conditions would greatly impact daily life and technology. Here, we focus on the multiatomic nature of a finite-size nanoparticle sliding on an atomically clean surface. The particle is subject to an effective field propagated by the surface and intermediated by the contact layer of the particle. The structural parameters, including the size, rigidity, and atomic configuration of the contact layer are taken into account to study the friction of the sliding nanoparticle. Several collective features show up once the particle contact layer is incommensurate with the surface potential, and the intralayer atomic coupling is strong. For a rigid layer, a considerable reduction of the friction is predicted at some particular sizes. In addition to these superlubric sizes that are determined by the lattice mismatch ratio only, enhancing the multiatomic feature by increasing the layer size and/or the intralayer coupling strength results in a friction reduction, which is essentially exponential for different values of the normal load (represented by the interaction amplitude). The latter kind of superlubricity is attributed to the increase of the number and synchronization of the intermediate slips of individual atoms in the contact layer that prevents the formation of high potential barriers. The edge atoms, on the other hand, are shown to be determinant in increasing the friction when they refuse to contribute to the collective slips.

DOI: 10.1103/PhysRevB.98.075407

I. INTRODUCTION

Friction is perhaps the most pervasive mechanical phenomenon in nature. Static friction is beneficial to our daily life by keeping surfaces stationary on each other. Kinetic friction, on the other hand, is a major source of wear of solid surfaces and energy loss into heat. The difference between the macroscopic and microscopic pictures of friction [1] manifests itself easily. Recall Coulomb and Amontons' laws: friction force is independent of contact area and sliding velocity but increases linearly with the normal load at the macroscopic interfaces. In contrast, friction between two atomic-scale surfaces does depend on the contact size and sliding speed [2,3] and varies nonmonotonically with load [4]. Compared to the macroscopic scale, better control and more details are accessible in friction experiments at the nanoscale. In particular, kinetic friction between macroscopic bodies is traditionally reduced by introducing lubricants into the contacts while a complete elimination of dry (i.e., no lubricant) friction has been realized at nanocontacts [5,6].

The intriguing state known as structural lubricity emerges at the atomically clean interface of two lattices if their relative orientation is set out of commensurate (locking) angles or if the ratio of the lattice parameters is an irrational number [5]. In the thermodynamic limit of an infinitely large interface, the frictional forces felt by the atoms of each surface overly sum up to zero due to translational symmetry under the incommensuration condition [7]. Thus, one may call this really frictionless and nondissipative motion the superlubricity (SL) state. Even under ambient conditions [8] or for finite-size contacts [9,10] the possibility of sliding with very low or negligible friction has been proven. Commonly, this ultralow friction state is categorized in the same family as the SL state to distinguish it from the high frictional stick-slip (SS) motion. This nonlinear phenomenon happens if the two surfaces remain stuck together until the external pulling force overcomes the static friction and breaks down the sticking state. The surfaces slip suddenly past each other and the stored elastic energy is dissipated, but they stick together again at a new relative position, and so on. This regular SS motion is highly frictional and dissipative, and is observed at almost any length scale: relative motion of the earth's plates [11], noisy scratching of chalk on a blackboard, peeling of an adhesive tape from the roller [12], dragging an atomically sharp friction force microscope (FFM) tip on a graphite surface [13], etc.

Investigating the difference between the two frictional regimes (SL and SS) from a microscopic viewpoint has attracted a considerable attention. The SL to SS transition on different model interfaces has been studied by playing around with several physical parameters. For example, it is shown that the dragging of a graphene nanoribbon on a clean metallic surface is frictionless [9] only if the ribbon is not longer than a critical length [14–16]. The SS motion is shown to be induced by, e.g., pinning the edges of the flake to the metallic substrate lattice [9,14,16–18], or by increased normal load on the FFM tip over NaCl surface [6]. Here, we aim to study the effect of the multiparticle nature of the nanocontact on its frictional behavior. In the rest of this paper, we first describe our atomistic model that reduces efficiently the complexity of the phenomenon by introducing an effective field within the adiabatic approximation. For asymptotically stiff or loose contact layer, analytic expressions for the frictional quantities are obtained. Then numerical results for arbitrary structural parameters are presented and a few interesting observations

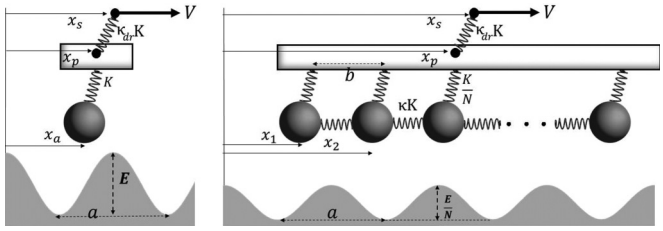

FIG. 1. Sketch of the model with point (left) or extended (right) apex. The particle has a rigid body (shown by a rectangular box), which is attached elastically to its apex on the bottom and to a moving support on the top. The large apex is composed of N (quasi)atoms, being subject to the surface potential with an amplitude normalized by N, and are connected to the particle body by N identical springs of relative stiffness $1/N$ while the intralayer relative stiffness is κ. The particle interacts via the apex with the substrate surface represented by a sinusoidal potential of periodicity a. The particle-support elasticity is $\kappa_{\rm dr}$ relative to that of the particle apex.

are discussed in comparison with the already-published experimental and theoretical results.

II. MODEL

A rigid support of instantaneous position $X_s = Vt$ drives a nanoparticle at constant speed V over a rigid surface, as illustrated schematically in Fig. 1. The sliding nanoparticle is flexible and consists of three components: (i) the particle body, (ii) a handle (cantilever) that connects the particle body to the rigid support, and finally (iii) the foremost atomic layer of the particle that is in an immediate contact with the substrate surface. The contact layer is represented by a one-dimensional (1D) chain of N atoms with mutual harmonic coupling of stiffness κK between the nearest neighbors only. (The dimensionless stiffness κ characterizes the lateral rigidity of the contact layer.) We denote the position of the centroid of the contact layer, referred to as apex hereafter, by $X_a \equiv \frac{1}{N}\sum_i X_i$, where $X_i[X_p(X_s)]$ represents the ith atomic position when the support is at position X_s and the particle body at X_p. So far, three central quantities are introduced as positions X_s, X_p, and X_a. For convenience, the arbitrary reference of the positions of the particle body and contact layer atoms are chosen such that the natural (i.e., in the absence of the substrate) values of the central quantities coincide $X_a^0 = X_p^0 = X_s$. A trivial choice for the contact layer is a regular lattice of spacing $b = (X_N^0 - X_1^0)/(N-1)$ so that the atomic rest positions become $X_i^0 = X_p + ib - (N+1)b/2$. A glassy structure can be obtained by introducing randomized distortions of given amplitudes to these positions.

To have comparable results with the conventional single-atomic models, we intend to keep the overall layer-to-particle stiffness equal to K independent of the number N of the atoms in the chain. Therefore, N identical springs, each of constant K/N, attach the N atoms of the contact layer to the particle body at positions X_i^0. In the absence of the substrate, no force is felt by the particle body from the apex as it is relaxed. When the contact layer is deformed due to interaction with the substrate, the force on the particle body from the layer is given by summing up all atomic contributions and reads $\frac{1}{N}K\sum(X_i^0 - X_i) = K(X_p - X_a)$. Note that this force is N independent as we imposed. The particle body is equilibrated if this force is canceled by the elastic force $\kappa_{\rm dr}K(X_s - X_p)$ exerted by the support via the elastic cantilever of an effective spring constant $\kappa_{\rm dr}K$ and instantaneous elongation $X_s - X_p$. At the moment, we do not restrict ourselves to the equilibrium state.

For a given support position X_s, the Lagrangian of our tricomponent model system, having $N+1$ degrees of freedom, reads

$$\mathcal{L} = \frac{1}{2}M_p\dot{X}_p^2 + \sum_{i=1}^{N}\frac{1}{2}M_i\dot{X}_i^2 - U(X_p; X_1, \ldots, X_N).$$

The potential energy is given by

$$U = \frac{\kappa_{\rm dr}K}{2}[X_p - X_s(t)]^2 + V_N(X_p; X_1, \ldots, X_N). \quad (1)$$

The first term represents the elastic contribution due to the cantilever deformation while the second term describes the interaction with the sample surface. We model the sample surface as a rigid atomic lattice of periodicity a that interacts with every atom in the contact layer via a sinusoidal potential of peak-to-peak amplitude E/N (if more than the first Fourier component of the surface potential are significant, they can be included in a similar way). The overall particle-surface interaction depends also on the size, atomic arrangement, and rigidity of the particle contact layer. More precisely, the effective surface potential energy

$$V_N = \frac{1}{N}\sum_{i=1}^{N}\left[-\frac{E}{2}\cos\left(\frac{2\pi X_i}{a}\right) + \frac{K}{2}\left(X_i - X_i^0\right)^2\right] + \frac{\kappa K}{2}\sum_{i=1}^{N-1}\left[(X_{i+1} - X_i) - \left(X_{i+1}^0 - X_i^0\right)\right]^2 \quad (2)$$

describes the interaction between the particle and the substrate intermediated by the N-atom contact layer by taking into account the collective response to the external shear strain by the layer atoms. The periodic term in V_N tends to put the atoms in the substrate potential wells by rearranging them into a lattice commensurate with the substrate, while the two elastic terms tend to keep the atoms in their natural positions X_i^0. For $N = 1$ (i.e., when the κ-dependent term is missing), this competition is usually characterized by the substrate corrugation parameter

$$\eta \equiv \frac{2\pi^2 E}{Ka^2}. \quad (3)$$

For finite sizes the multiatomic parameters come into play, too. For example, arguing that all the springs connected to the layer atoms act simply as they are in parallel, one may replace K by $N(K/N) + (N-1)\kappa K$ to obtain

$$\eta_{\rm N} \sim \frac{\eta}{1 + (N-1)\kappa}.$$

The argument is, however, not valid because not only the many-body nature and collective response of the atomic layer are completely ignored, but also it is assumed that all the atoms experience identically the surface potential, i.e., the layer and surface lattices match perfectly. In general, the misfit parameter $m \equiv b/a$ is not an integer and the effective corrugation

becomes N and m dependent (and perhaps unrepresentable analytically in general) as will be explored in Sec. III A.

Units. Hereafter we take $a/2\pi$ as the length unit and $Ka^2/4\pi^2$ as the energy unit. Then the unit of force is $Ka/2\pi$, see Eqs. (4)–(6). For experimentally relevant values $a = 3.14$ Å and $K = 1$ N/m (known as tip stiffness in FFM experiments), we have $Ka/2\pi = 50$ pN and $Ka^2/4\pi^2 = 0.031$ eV so that $\eta = 1$ corresponds to a substrate corrugation $E = 0.62$ eV. It would be reasonable to limit our investigation to the range $1 < \eta < 20$. Note that $\kappa_{\rm dr} \sim 10$–100 corresponds to typical cantilever stiffnesses in FFM experiments. In a previous work, we have estimated the stiffness per unit for a C-C bound molecular chain by calculations based on different approximations to the density functional theory to be $\kappa \sim 250$–575 [19]. For bulk crystals, one can show that the Young's modulus (∼5–300 GPa) times the interatomic equilibrium distance gives the interatomic spring constant (∼1–150 N/m). We therefore sweep κ with logarithmically increasing steps up to 500.

Nondimensionalization. Solving numerically the equations by implementing a computer program is more convenient if the quantities are dimensionless. This also leads to conveniently express the equations without repeating constant factors. For example, instead of the lattice constant a, one works with the dimensionless periodicity of the surface potential, which is 2π when the length unit is $a/2\pi$. We will use throughout this study the dimensionless length, potential energy, and force defined as

$$x_\alpha \equiv \left(\frac{2\pi}{a}\right) X_\alpha, \tag{4}$$

$$v_N \equiv \left(\frac{4\pi^2}{Ka^2}\right) V_N, \tag{5}$$

$$f_\alpha \equiv \left(\frac{2\pi}{Ka}\right)\frac{\partial \mathcal{L}}{\partial X_\alpha} = -\frac{\partial v_N}{\partial x_\alpha} - \frac{\kappa_{\rm dr}}{2}\frac{\partial}{\partial x_\alpha}(x_p - x_s)^2, \tag{6}$$

where $\alpha = s, p, a, i$ for support, particle, apex, and atomic coordinates, respectively.

III. RESULTS AND DISCUSSION

The goal of this study is to explain the frictional behavior of the nanoparticle sliding on the periodic surface. The first approach is based on exploring the dependence of the effective surface potential

$$v_N(x_p; x_1, \ldots, x_N) = \frac{1}{N}\sum_{i=1}^{N}\left[-\eta\cos x_i + \frac{1}{2}\left(x_i - x_i^0\right)^2\right] + \frac{\kappa}{2}\sum_{i=1}^{N-1}\left[(x_{i+1} - x_i) - \left(x_{i+1}^0 - x_i^0\right)\right]^2 \tag{7}$$

on the multiatomic parameters of the apex layer (N and κ) and the misfit and corrugation parameters (m and η). The internal degrees of freedom of the particle apex are accumulated in the field

$$v_N(x_p) \equiv \min_{x_1,\ldots,x_N} v_N(x_p; x_1, \ldots, x_N)$$

that gives the potential energy as function of the particle-body position x_p when all atoms of the apex layer are relaxed to their optimum positions that minimize the potential energy. In general, the minimization is performed iteratively using a numeric approach. We will first address particular cases that can be treated analytically and derive compact expressions useful to shed some light on the problem of friction between extended contacts and to interpret some numeric results obtained later on. Subjecting the pointlike assumed particle body to this field, the interaction with the surface via the multiatomic apex of the particle is fully described, while one plausibly keeps using the formalism of the basic single-particle models.

A. Superlubric sizes

If the apex is a regular atomic lattice of lattice constant b, one sees that $x_i^0 = x_p + [2i - (N+1)]m\pi$ (obtained by dividing the atomic rest positions given in Sec. II by the length unit $a/2\pi$ to become dimensionless and recalling that $m = b/a$). In the limit of strongly coupled atoms to the particle body, or equivalently weakly interacting atoms with the substrate surface, i.e., when $K \gg E/a^2$, the constraint $x_i = x_i^0$ suppresses the internal degrees of freedom and only the cosine term in Eq. (7) is nonzero. For such a rigid particle, the particle-substrate interaction takes the trivial form of sinusoidal potential, namely

$$\lim_{K\to\infty} v_N = -\frac{\eta}{N}\sum_{i=1}^{N}\cos x_i^0 = -\eta_N^{\rm rigid}\cos x_p,$$

where the effective corrugation parameter reads[1]

$$\eta_N^{\rm rigid} = \left(\frac{\sin Nm\pi}{N\sin m\pi}\right)\eta.$$

Similarly, for a highly stiff chain $\kappa \gg 1$, a rigid shift of $x_i - x_i^0 = x_a - x_p$ is induced to every atomic position and the apex-intermediated potential of the substrate affecting the particle body reads

$$\lim_{\kappa\to\infty} v_N = -\eta_N^{\rm rigid}\cos x_a + \tfrac{1}{2}(x_a - x_p)^2. \tag{8}$$

The interpretation is interesting, specially to understand why the simple and basic models that assume the tip apex to be a single atom (see Sec. IV) have been fairly successful to explain many experimentally observed nanofriction results for FFM tips [5,6]. Comparing Eqs. (8) and (13), we conclude that two nanoparticles, one with an extended rigid apex layer whose centroid position is x_a and one with a single-atom apex at position x, both being subject to the same surface periodic potential of corrugation η, are governed by identical mathematical equations but the effective corrugation appeared to the nanoparticle with the extended apex is $\eta_N^{\rm rigid}$. First, for

[1]Note that $\sum_{n=1}^{N} e^{Jn\alpha} = \frac{1-e^{JN\alpha}}{1-e^{J\alpha}} = \left(\frac{\sin N\alpha}{\sin\alpha}\right)e^{J\left(\frac{N-1}{2}\right)\alpha}$, where $J = \sqrt{-1}$.

$m = 1$ (i.e., perfect lattice matching $a = b$) the ratio $\eta_N^{\text{rigid}}/\eta = \sin(Nm\pi)/(N \sin m\pi)$ reaches the bounding values ± 1, becomes N independent, and results in the maximum friction force. (The ratio equals -1 for an even number of atoms meaning that the pinning position of the particle body is shifted by $a/2$ compared to the case of an apex with one or any odd number of atoms.) We conclude that if the nanoparticle has a rigid apex layer with a periodicity equal to the surface potential periodicity, the apex layer is equivalent to one single atom.

Now we consider the case that the lattice of the rigid apex misfits the surface potential (m is noninteger), for which one sees that the effective corrugation amplitude is reduced by a factor $\sin(Nm\pi)/(N \sin m\pi) < 1$. The factor vanishes if $\sin(Nm\pi) = 0$, i.e., when the layer size satisfies $N = p/m$ with p being an integer. For example, for a commensurate layer with $m = 5/4$ the corrugation vanishes (and superlubricity is gained) at sizes $N = 4, 8, 12, \ldots$. Even for incommensurate lattices (irrational m), the factor (and thus the corrugation η_N^{rigid} and the friction force) becomes small depending on how close to an integer Nm is. For instance, if the mismatch ratio equals the golden mean $m = (\sqrt{5}+1)/2$, the sizes of relatively small corrugation are $N = 3, 5, 8, 13, 21, \ldots$, i.e., Fibonacci numbers. This prediction is supported by our numerical results (see high-κ branches in Fig. 3). For any rational or irrational mismatch ratio there exist such particular lengths that result in small effective corrugation amplitude. To get a pinned or a smoothly sliding state of a tightly bound chain of atoms on a periodic surface, one should consider these particular numbers of atoms.

In the opposite limit of noninteracting atoms $\kappa \simeq 0$, a reduced form of Eq. (7) is obtained as

$$\lim_{\kappa \to 0} v_N = -\eta \langle \cos x_i \rangle_N + \tfrac{1}{2} \langle (x_i - x_i^0)^2 \rangle_N,$$

where $\langle . \rangle_N$ denotes averaging over N atomic contributions. If additionally the layer-surface fitting is perfect (m is an integer) the individual atoms are statistically independent. Physically, this means that all atoms are replicas of a single one and no multiatomic feature appears. In particular, at finite temperatures $\langle . \rangle_N$ denotes averaging over N replicas of a single atom that differ only in thermal fluctuations, as will be discussed in more detail in Sec. IV B in connection with the model introduced by Maier *et al.* [20]. Collective features show up once m is not an integer because the atoms are attached to a common base on the particle body even though they lack a direct mutual coupling $\kappa = 0$.

As illustrated in Fig. 1, the interactions of each atom with the surface and the particle body both are scaled by N in our model. So, for any value of N, the ratio η characterizes the competition between the surface corrugation and the apex-body stiffness and determines whether the atoms remain close to their unperturbed positions x_i^0 on the particle body and slide smoothly on the surface (as a rigid layer that was discussed above) or fall down into the wells of the substrate potential energy surface to experience a high frictional sliding. For a moderate η, the unbound atoms are expected to move incoherently and contribute, by a nonconstructive superposition, to $\langle \cos x_i \rangle_N$ to make $v_N(x_p)$ a rugged function of the particle position. Over such an irregular energy landscape, there exist many shallow local minima that might or might not be sticky enough to trap the particle. The final state depends also on multiatomic parameters N and κ. A quantitative exploration of this issue and finding the critical corrugation parameter, is possible in terms of the concavity of potential energy surface (PES). The concavity is a measure of the local curvature of a high-dimensional PES and is useful to characterize the stability nature of the equilibrium points on it. If the PES is concave at some (equilibrium) configuration, the particle is confined there. For a given particle position, the PES, given by Eq. (7), is a function of N coordinates of the contact atoms. The second partial derivatives of the PES are collectively represented as the $N \times N$ Hessian matrix $\mathbf{k}_{ij} = \partial_{x_i x_j} v_N$ which reads

$$\begin{pmatrix} (\chi_1 + \kappa) & -\kappa & & & \\ -\kappa & (\chi_2 + 2\kappa) & -\kappa & & \\ & & \ddots & & \\ & & -\kappa & (\chi_{N-1} + 2\kappa) & -\kappa \\ & & & -\kappa & (\chi_N + \kappa) \end{pmatrix}.$$

For an unbound ($\kappa = 0$) chain of atoms, the Hessian matrix is diagonal $\mathbf{k}_{ii} = \chi_i = (\eta \cos x_i + 1)/N$ where $\chi_i = \frac{1}{N}(\eta \cos x_i + 1)$. Then, neither of the matrix eigenvalues are negative (meaning that the energy landscape is strictly concave) if $\eta < 1$. This results in a superlubric smooth sliding of the particle. For $\eta > 1$, on the other hand, eigenvalues of the Hessian matrix may take a negative sign, and thus a stick-slip behavior is expected. Indeed, atom i experiences a slip event if the eigenvalue χ_i is zero, which occurs at position $x_i^c = \arccos(-\eta^{-1})$.

If κ is finite, the subdiagonal elements (the only nonzero off-diagonal elements, corresponding to the nearest-neighbors interactions throughout the chain) modify the eigenvalue spectrum. the critical corrugation parameter would also deviate from one. This complicated case has to be treated numerically, as done later on.

B. Size and stiffness dependence of friction

The natural outcome of a nanofriction measurement, namely the instantaneous friction as a function of the support position, has the theoretical analog $F_s(X_s) = (\frac{Ka}{2\pi}) f_s(x_s)$. Plugging Eq. (7) into Eq. (6) with $\alpha = s$, one gains

$$f_s(x_s) = \kappa_{\text{dr}}[x_p(x_s) - x_s].$$

As the support advances, to calculate the friction force one needs only to determine the particle-body position x_p, which is in turn determined by the potential energy landscape $v_N(x_p)$ that is suggested by the substrate surface to the particle body but also intermediated by the particle-apex layer. Assuming that the system is in a quasisteady state, the net force on the particle body and those on the individual atoms in the contact layer are required to be zero (note that the our model system has $N + 1$ degrees of freedom). Nullifying the force on the particle body given by

$$f_p = \kappa_{\text{dr}}(x_s - x_p) + (x_a - x_p) \tag{9}$$

makes the particle equilibrated between its contact layer (apex) and the support so that the friction force may be expressed in

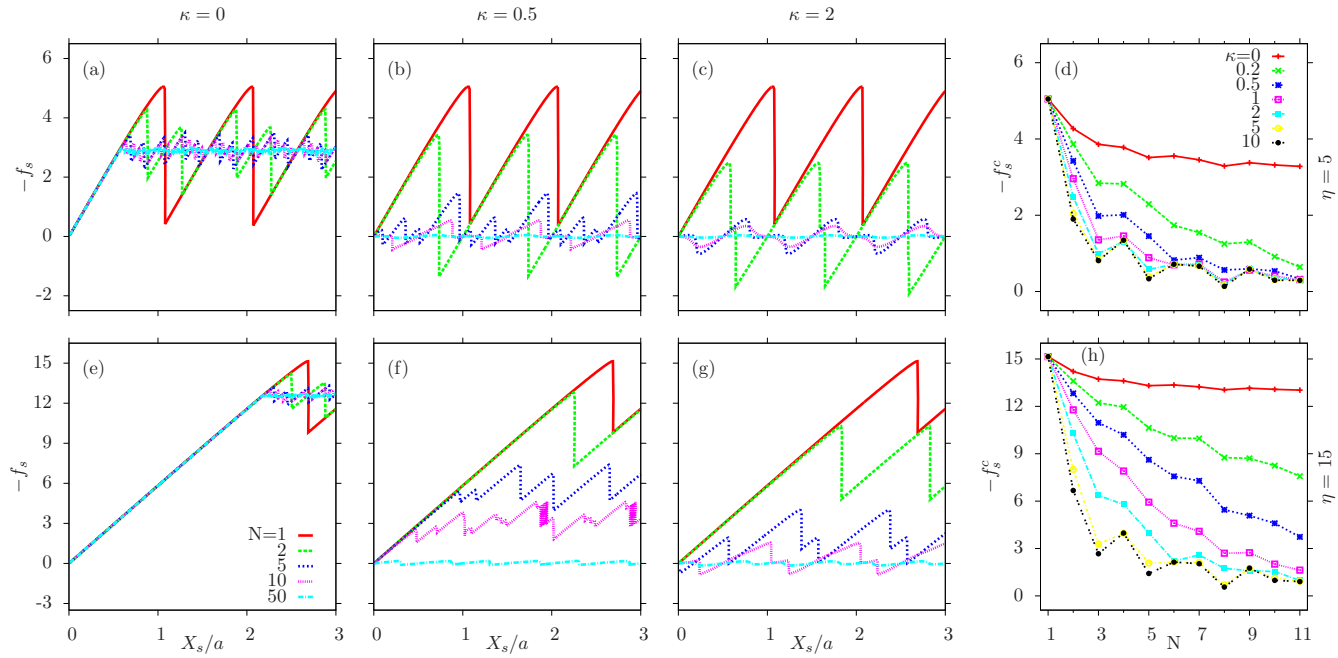

FIG. 2. Friction force, $-f_s$, as a function of support position for several chain lengths $1 \leqslant N \leqslant 50$ and bonding strength (a) $\kappa = 0$, (b) 0.5, and (c) 2, and (d) its maximum value $-f_s^c$ as function of chain length for $m = (\sqrt{5}+1)/2$ and $\eta = 5$. Bottom row: same as top row but for $\eta = 15$.

terms of either of the corresponding elongations as

$$f_s(x_s) = \kappa_{\rm dr}(x_p - x_s) = x_a - x_p. \tag{10}$$

Note that the normal ordering $x_a \prec x_p \prec x_s$ corresponds to a negative (resistant) f_s, while $f_s > 0$ implies that the apex leaves behind the body centroid (and similarly the body centroid overtakes the support reference position).

On the other hand, nullifying the net force on each of the layer atoms

$$f_i = -\tfrac{1}{N}\left(\eta \sin x_i + x_i - x_i^0\right) + \kappa d_i \tag{11}$$

implies that the atomic positions satisfy $x_i - x_i^0 = -\eta \sin x_i + N\kappa d_i$, where d_i denotes the difference between the elongations of the interatomic springs on the right and left of atom i. If all natural interatomic spacings are equal to b, one obtains $d_i = (x_{i+1} - 2x_i + x_{i-1})$ for the interior atoms, while $d_1 = x_2 - x_1 - 2\pi m$ and $d_N = x_{N-1} - x_N + 2\pi m$ for the chain ends. Since by definition $\sum_i^N d_i = 0$, the right-hand side of Eq. (10) is rewritten as

$$f_s(x_s) = \left\langle x_i - x_i^0 \right\rangle_N = -\eta \langle \sin x_i \rangle_N.$$

So far, we have discussed a number of asymptotic frictional behaviors of the nanoparticle based on analytically derived expressions. Trends and further interesting results are obtained by solving numerically the equations of motion of the model multiatomic system. For an arbitrary set of parameters (N, κ, η, m), one needs to find the roots of $f_p = f_i = 0$, i.e., the equilibrium configurations. Although it should not be so complicated to do this task on computer, the determination of the true transition path through the $(N+1)$-dimensional configuration space from the knowledge of the roots positions is not straightforward. Instead, the dynamics of the system is usually simulated by integrating the Langevin equation of motion in time. In this work we employ an efficient alternative for finding the true path with much less computational labor, as introduced in Appendix A.

The variation of the friction force versus support position calculated by Eq. (10) with a maximal incommensuration $[m = (\sqrt{5}+1)/2]$ for several values of N and η, is shown in Fig. 2 in three columns corresponding to three values of κ; for the sake of convenience, $-f_s$ is plotted versus x_s because the friction usually opposes the motion direction. The observed well-known sawtooth pattern is a signature of the stick-slip motion. The plots are curvy around the maxima due to the gradual disappearance of the well when the support advances. More precisely, the slip takes place when the well minimum and the adjacent barrier maximum converge to a same critical point x_c where the static friction reaches its maximum value f_s^c and the particle sets off the vanished well. The maximum friction force f_s^c averaged over 50 stick-slip cycles is plotted as a function of chain size in the fourth column. The plots show that the frictional behavior is strongly influenced by the contact size and interatomic bonding for both investigated corrugations. The duration of the sticking state and accordingly f_s^c decrease as either of the multiatomic parameters N and κ increase. At the same time, the curvy feature dominates the sawtooth pattern so that the stick-slip motion transforms to smooth sliding. This can be attributed to the broadening of the adhesion sites (to which the atoms stick) when κ increases at a fixed N, so that the forbidden regions between these sites become smaller and thus the sticking duration is shorter. When the number of atoms increases at a given κ, indeed the number of intermediate slips increases. Both of these effects prevent the formation of high potential barriers. This intuition is confirmed by the fact that the effect of increasing

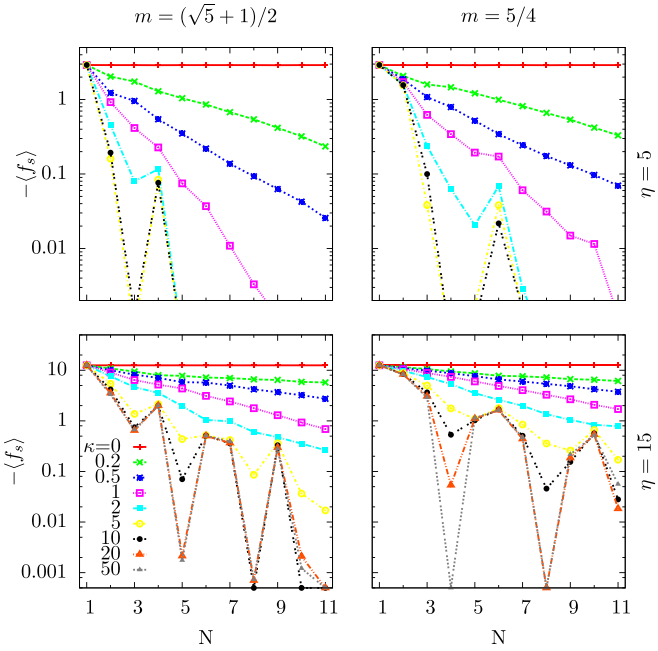

FIG. 3. Mean friction versus the number of atoms in the contact layer for different values of κ, for an incommensurate (left) or commensurate chain (right) with $\eta = 5$ (top row) and $\eta = 15$ (bottom row).

the corrugation parameter η opposes the effect of increasing N and κ, as seen in the bottom row. The surface corrugation tends to separate out the atoms and rearrange them as independent atoms in a lattice commensurate with the surface potential, while enhancing κ tends to keep them coupled together and behave collectively.

To better inspect the N and κ dependence of friction, the variation of the mean, i.e., time-averaged friction force $-\langle f_s \rangle_t$ as a function of the chain length is shown in a semilogarithmic scale in Fig. 3. The time-averaged friction corresponds to kinetic friction force, which is a relevant physical quantity. It is calculated as (we drop the subscript t for convenience)

$$\langle f_s \rangle \equiv \lim_{\tau\to\infty} \frac{1}{\tau} \int_0^\tau f_s(x_s(t))dt$$
$$\simeq \frac{a}{2\pi L} \sum_{k=1}^{n_k} f_s\left(x_s^k\right) \Delta x_s^k.$$

The summation approximates the work done by the external force to pull the support in n_k random steps Δx_s^k.[2] Based on trial and error tests, we were convinced that a line scan of length $L = (\frac{a}{2\pi}) \sum_{k=1}^{n_k} \Delta x_s^k \sim 50a$ is long enough to converge to steady-state values. As seen in all panels of Fig. 3, and discussed above, the kinetic friction force is essentially reduced when N and/or κ increase. There is an exception, however, in the extreme case of independent atoms $\kappa = 0$ (see also the left column of Fig. 2), for which the friction mean remains, for any value of m and η, unchanged for all chain lengths. The static friction force f_s^c, however, decreases slowly with N even in this exceptional case; see the $\kappa = 0$ branches in the right column of Fig. 2.

As soon as the intralayer atomic interaction is turned on, the kinetic friction decreases with N. The behavior is qualitatively similar for $\eta = 5$ or 15 (top and bottom rows in Fig. 3) but weaker corrugation causes smaller friction, in general. This leads to the conclusion that surface corrugation competes the multiatomic parameters (size and interatomic binding strength) that tend to reduce the friction, in consistence with our earlier intuitive argument based on the incoherent individual slips throughout the chain. Finally, note that for small κ, kinetic friction force decreases monotonically (exponentially) with N, but becomes vanishingly small at some particular sizes for strongly bound atoms. The plots for incommensurate and commensurate chains, shown on the left and right columns, seem fairly similar apart from these superlubric sizes. The presence and values of such superlubric sizes are already predicted in Sec. III A, in terms of the vanished amplitude of the effective potential v_N (or equivalently the effective corrugation η_N^{rigid}) for rigid chains.

C. Atomic configuration and edge effects

The deviation of the effective potential v_N from the naive sinusoidal potential of a single atomic apex is a result of local deformations throughout the multiatom contact. Clearly, plotting the whole local deformations (atomic displacements $\delta_i = x_i - x_i^0$ or bond elongations $d_i = \delta_{i+1} - \delta_i$) for the simulation time makes the plots too messy if not unreadable. We visualize the geometry of the chain by folding it into the unit interval using the Aubry's hull function [21]

$$h(X) = \frac{X}{a} - \left\lfloor \frac{X}{a} \right\rfloor, \tag{12}$$

which measures distances relative to the closest lattice node on the left. One essential feature of this representation is that a discontinuity (known as analyticity breaking) in $h(X)$ corresponds to a slip event along the X coordinate and implies a gap in the excitation spectrum of that component. In contrast, a continuous diagram corresponds to low frictional smooth sliding and corresponds to a superlubric state.

First, we compare in the following two representative short chains of lengths $N = 3$ (recall that the Fibonacci number 3 is a superlubric size when m is set to the golden mean) and $N = 4$, which exhibit pronounced κ-dependent frictional behavior, as seen in Fig. 3. We consider in our experiment only three values of stiffness $\kappa = 1, 2, 5$ with distinct differences for both triatomic and quadatomic chains. The profile of the hull function diagram for the triatomic chain, shown in Fig. 4, alters significantly upon increasing κ: the number of gaps and their widths reduce and finally a discontinuous-to-continuous transformation, corresponding to SS-to-SL transition takes place. In contrast, the quadatomic chain's hull diagram, shown in Fig. 5, remains singly gapped and its profile remains essentially unchanged over the same range of κ. The position of each of the four atoms in the quadatomic chain spans only almost one half of each lattice spacing while the other half is always slipped over. This large gap is an indication of a high-frictional SS motion, in agreement with Fig. 3 (left column). It is worth noting that the slips of the four atoms are

[2]Higher-order approximations to the integral are not helpful when the step length is chosen randomly.

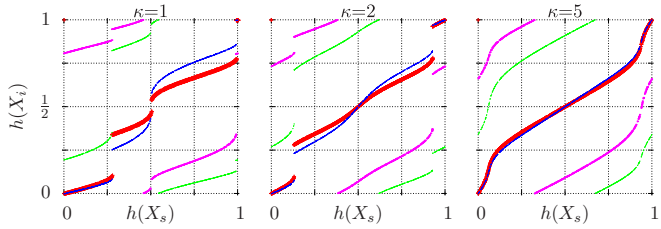

FIG. 4. Representation of atomic configuration based on the hull function, Eq. (12), for a chain of length $N = 3$. The pronounced (red) branch corresponds to the chain's center of mass while the thin ones to the atoms. The interatomic stiffness κ increases from left to right, $m = (\sqrt{5}+1)/2$ and $\eta = 5$ [same as in Fig. 3(a)]. Data points are collected for a line scan of length $50a$.

synchronized with each other and thus with the chain's center of mass (CM). Note how the broken branches of different atoms are connected together in the hull diagram; as soon as an atom leaves an adhesive site on the surface, the atom behind it sits immediately at that site; As a result, the chain follows the support by a high-frictional SS motion.

Next, we plot in Fig. 6 the hull diagram for another incommensurate but longer ($N = 10$) chain. Compared to the short chains, superlubricity is gained for much smaller stiffness κ. Moreover, the individual atoms slip in turn and asynchronously when they are independent ($\kappa = 0$) or not tightly bound ($\kappa = 0.2$). The resulting hull function of the CM shows ten, i.e., the same as N, small gaps while the discontinuities of the atomic hull functions, i.e., the length of the individual slips, is much longer ($\sim 3/4$ and $\sim 1/4$, for $\kappa = 0$ and 0.2, respectively), which is also seen in the corresponding plots in the bottom row where the hull function of individual atomic positions are plotted separately. By increasing κ, the number of gaps of the CM branch decreases. For $\kappa = 0.5$, many atomic slips disappear while some others become synchronized such that only two gaps are survived on the CM hull function. The ordering of the branches, needed to identify the atomic slips that are synchronized, is deduced by comparison with the panels on the bottom row. The sum of the CM gap widths is smaller and results in a decreased mean friction, as expected from Fig. 3. By inspecting the hull function of individual atoms, shown on the bottom row, we found that the largest slips belong to the atoms at or close to the chain ends. In other words, the atoms at the edges of the layer can suppress the superlubricity by sticking to the sample surface and slipping over rather long distances. This is in complete agreement with the previously reported observation for dragging one end of a single-atom thick molecular layer adsorbed on crystalline surfaces [14]. The atoms at the free edges are more flexible

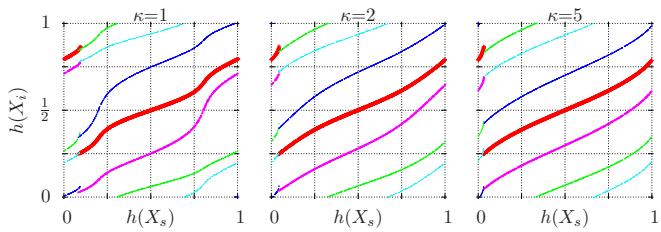

FIG. 5. Same as Fig. 4 but for length $N = 4$.

than the inner atoms and thus have a higher chance to become pinned to surface confining sites. Studying the same effect at the position of a defect (a missing atom, for example) to see whether it induces similarly high-frictional stick-slip motion merits further experimental investigations. Finally, recall that friction mean was shown in Fig. 3 to decrease when the number of atoms and/or their mutual binding strength increases. We attributed this to the increment of the individual atomic slips and extension of the adhesion sties. This intuitive argument is confirmed by looking directly at the atomic configurations represented in the hull diagrams.

For stiff chains ($\kappa = 1, 2$) the sliding becomes smooth and frictionless, as all atoms including edge and inner atoms slide continuously without getting pinned to the surface. The high-κ hull diagrams look fairly symmetric with respect to the central point, implying the time-reversal property: if the support motion direction is reversed, the trajectory remains unchanged. In contrast, low-κ plots are asymmetric so that hysteresis loops would be generated if the support goes backward to the starting point. Indeed, the symmetry of the hull diagrams is another signature of the smooth sliding. To conclude, for bound atoms in the contact layer, apart from the particular superlubric sizes satisfying $N \sim pm$, where p is an integer, the friction tends to decrease as the chain becomes longer and stiffer.

IV. RELATION TO FFM

There are three characteristic types of elastic connection between the components of our model illustrated in Fig. 1 and described by Eqs. (1), (2): The particle-support connection has a spring constant $\kappa_{\rm dr}K$, the overall stiffness of the particle-apex connection is K (which is distributed among N identical springs of constant K/N), and the flexible apex is a layer with interatomic springs of constant κK. Replacing one or some of these elastic connections with rigid bonds simplifies the model, and probably reduces it to one of the previously proposed models by other researchers. Our discussion in the following mainly concerns the question that why and when an elastic term is really required to be explicitly taken into account.

Traditionally, the basic and simplest framework to describe the stick-slip motion at an atomic scale has been the Prandtl-Tomlinson (PT) model [22,23]. This model successfully describes several aspects of experimentally observed frictional behavior of sliding FFM tips or nanoparticles on a periodic surface. This success is somewhat surprising because the tip asperity is not guaranteed to be a single atom but in most experiments the frontmost atomic layer that is in immediate proximity to the substrate surface contains several atoms while the PT model considers the tip to be a structureless particle. Modeling the apex as a chain of bound atoms as explained above, is indeed a first step to take into account the multiatomic nature in a simple way. The appealing feature of the developed framework, that can be considered as an extension to the PT model, is that while the simple formalism of the conventional PT model is preserved, the tip position-dependent structure of the particle apex is convolutionally encoded into a single effective potential $v_N(x_p)$, Eq. (7). It is instructive to clarify in more detail how our model is connected to the PT model, and also to compare it with the extensions to the PT model developed previously for FFM investigations.

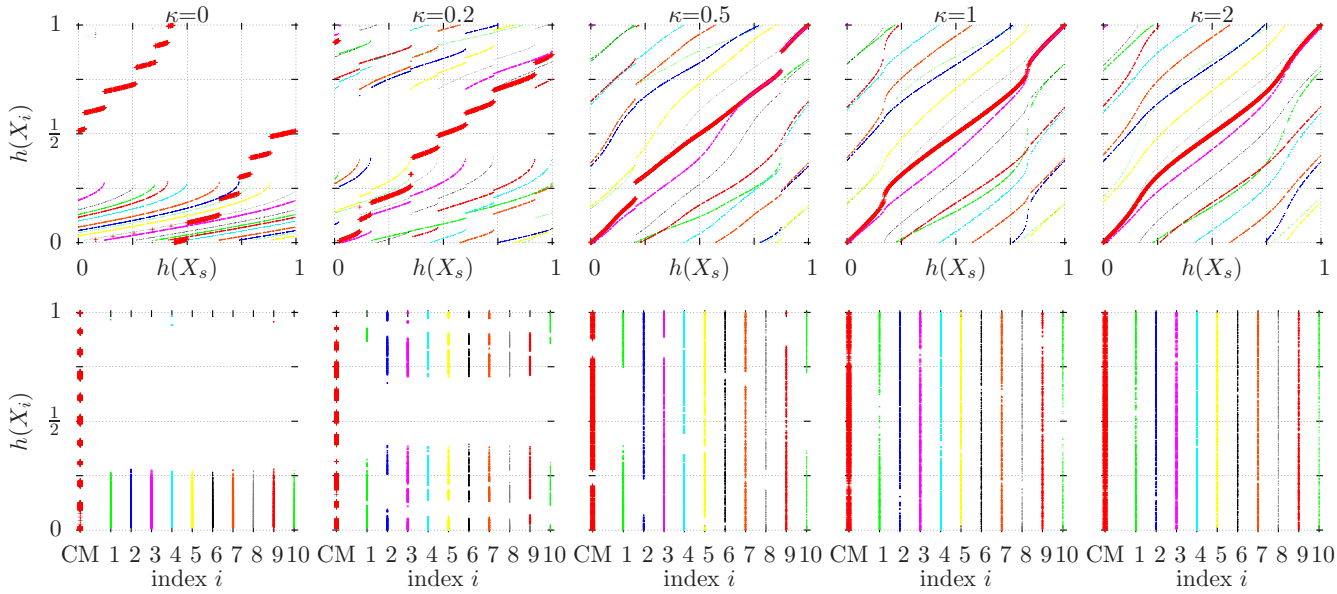

FIG. 6. Same as Fig. 4 but for length $N = 10$. Bottom row: Hull function of the center of mass, and individual atomic positions as a function of their index.

A. Point apex and rigid lever

In early studies based on the primitive PT model, the FFM tip was modeled as a pointlike particle of some effective mass, which is dragged through a corrugated substrate surface. The PT particle (FFM tip) is indeed a single-atom apex ($N = 1$) attached (via spring K) to the particle body. Analogous to the configuration vector $\mathbf{x}$ in our formalism, the apex position is always $x = x_a$, so that Eq. (7) is reduced to

$$v_1 = -\eta \cos x + \tfrac{1}{2}(x - x_p)^2. \tag{13}$$

Note that our effort so far was meant to generalize v_1 to v_N in order to include finite-size and interatomic bonding of a flexible apex.

The particle body in the PT model is rigidly ($\kappa_{\rm dr} \gg 1$) attached to the support ($x_p = x_s$). Plugging v_1 into Eq. (1), the potential energy reads

$$U_{\rm PT} = V_1 = \left(\frac{Ka^2}{4\pi^2}\right)\left[-\eta \cos x + \frac{1}{2}(x - x_s)^2\right]. \tag{14}$$

The PT particle tends to relax to an energy minimum to feel no force $F = -\partial_X U_{\rm PT} = -(\frac{Ka}{2\pi})f$, where

$$f = -(\eta \sin x + x - x_s) \tag{15}$$

is the monatomic analog of the force vector $\mathbf{f}$ with components given by Eq. (11). The number of stationary points of the energy, i.e., the solutions to equation $x + \eta \sin x = x_s$ characterizes the frictional behavior of the PT particle. This number depends on the surface relative corrugation, Eq. (3). If the local curvature of the energy surface $\partial_{XX} U_{\rm PT} = K\chi$ is strictly positive then $U_{\rm PT}$ has no corrugation and is confining everywhere so that the particle slides smoothly on it. Recall that $\chi = \eta \cos x + 1$ is analogous to the diagonal elements of the Hessian matrix when the apex contains more than one atom. A positive curvature $K\chi$ corresponds to $\eta < 1$, i.e., weak substrate interaction or stiff cantilever. On the other hand, for $\eta > 1$ the energy potential surface becomes corrugated and contains successive hills and valleys (where χ is negative and positive, respectively). As the support advances, the particle resides in a valley minimum, which satisfies $\eta \sin x + x = x_s$. The instantaneous friction force [see Eq. (6)]

$$-f_s = x_s - x = \eta \sin x \tag{16}$$

grows almost linearly with x_s for a large range because x increases very slowly with increment of x_s so that $-f_s \simeq x_s$. In the same time, the x_s-dependent parabolic contribution to Eq. (14) is shifted with respect to the sinusoidal one such that the Peierls-Nabarro (PN) barrier height (the energy difference between the hill maximum and the valley minimum) decreases. Once these two extrema converge to a same point $x^c = \arccos(-\eta^{-1})$, which is called a critical point because $\chi = 0$, the particle sees no PN barrier. The critical friction $-f_s^c = \eta \sin x^c = \sqrt{\eta^2 - 1}$ is the maximum (static) friction force that the particle can exert on the support against its motion, and beyond which the particle slips to stick to the next well minimum.

As seen in the $N = 1$ branches in Fig. 2, near the critical point $f_s(x_s)$ becomes curvy because the approximation $x_s - x \simeq x_s$ is no longer valid. After slipping to the next minimum $x_s - x$ and thus $-f_s$ become small or even negative. These all resemble the SS motion. At zero temperature, the SS-SL transition occurs critically at $\eta = 1$, which distinguishes corrugated from smooth landscapes. For motion with a sufficiently low speed, the stored energy in the stick phase is transformed into kinetic energy upon slipping and then completely damped as phonons into the substrate (and probe). At finite temperature, or if the support moves so fast that the slipped particle would not fully relax before the new PN barrier vanishes, the particle overcomes hills of finite height. This suggests that increasing the speed or temperature reduces the friction in agreement with the experimental observations [2,24].

B. Point apex and elastic lever

The primitive PT model predicts a sudden jump over PN barriers. One subtle effect that this simple model fails to describe is the finite duration of the slip event detected in experiment [20]. Maier *et al.* represented the tip apex by multiple asperities and showed that the slipping phase becomes smoothened and takes a while (see Figs. 5 and 6 of Ref. [20]) due to incoherent jumps of the individual asperities. Each of the N asperities is attached elastically by a spring of stiffness K/N to a common tip body, which is in turn connected elastically to the support. Our model is indeed inspired by this idea but we additionally include the interasperity coupling and did not delimit the mismatch parameter to integers. In contrast, they set the equilibrium distance between the asperities equal to (indeed, commensurate with) the substrate periodicity to be able to observe the substrate periodicity. The asperities in their model are not directly coupled together and thus it works in practice as an average of multiple replicas of a PT particle that are statistically independent and differ merely in thermal fluctuations. The essential element in their model, without which one cannot get the slip prolongation, is taking into account the elasticity of the cantilever.

Explaining the slip prolongation is possible also in terms of delocalization of the tip apex between potential energy wells, as proposed by Abel *et al.* [25]. The CM of the tip is connected by a stiff spring to the support but also by a loose spring to the tip apex that interacts with the periodic substrate surface. The latter spring represents the flexibility and slippery nature of the contact. For a given support position, a time average of the apex position (or any quantity) is indeed a weighted one over all possible apex positions.

The two extensions to the PT model cited above are essentially identical in the sense that both of them are averaged double-spring PT models. By double-spring we mean that both particle-support and particle-apex connections are elastic (in contrast to the basic PT model where the particle-support connection is rigid). Including this degree of freedom is critical in the occasion addressed above. The averaged double-spring PT model is gained by taking an average either over the time (as in Abel's extension) or over a set of replicas that are identical unless in thermal randomization (as in Maier's extension). In our notation, both of these extensions are simply obtained by replacing $V_N \leftarrow \langle V_1 \rangle$ in Eq. (1), namely

$$U_{\mathrm{PT2}} = \frac{\kappa_{\mathrm{dr}} K}{2}(X_p - X_s)^2 + \langle V_1 \rangle, \tag{17}$$

where $V_1 = Ka^2/(4\pi^2)v_1$ is given by Eq. (13).

C. Extended flexible apex

The Frenkel-Kontrova (FK) model is widely used to describe the dynamics of a chain of mutually interacting particles subject to a periodic potential [26] in a rich variety of physics problems from dislocations and charge density waves in solid crystals to trapped cold ions in optical lattices [27,28]. A variant of the FK model, where the foremost atom of the atomic chain is harmonically connected to a rigid moving support, successfully explains the SL state observed experimentally for a graphene nanoribbon over gold surface [9]. It was also used to show that either pulling or pushing the chain results in an SL to SS transition at certain chain lengths [15]. The potential given by Eq. (7) adopts the same idea to be applicable to nanoparticles thicker than a monolayer by connecting all the atoms to the particle body. Apart from the finite size of the chain, and including the body-support elastic connection, our model is reminiscent of a previously studied model called the Frenkel-Kontrova-Tomlinson (FKT) model [29,30]. The edges and the additional spring, both ignored in the FKT model, can become critically determinant in friction [14,20,25].

V. CONCLUSIONS

The very simple Prandtl-Tomlinson model has been very successful in explaining many experimental nanofriction observations in either stick-slip or a smoothly sliding (superlubricity) regime [5,6]. This is surprising because this model assumes the sliding object to be pointlike (i.e., its lateral extension is ignored compared to the periodicity of the potential of the surface) while the apex of a friction force microscope tip is not guaranteed to carry a single atom at its very end. Inspired by this fact, we seek to construct a theoretical framework that enjoys the simplicity of the commonly used and well-studied single-particle PT model, and at the same time be applicable to nanocontacts of sizes larger than a single atom. By conceptually separating the flexible apex layer from the rest of a nanoparticle, a notable methodological simplification is obtained: the equation governing the sliding motion of the nanoparticle is reduced to the simple form of the PT model at the expense of replacing the sinusoidal particle-surface interaction with an effective field. The particle body, which resembles the pointlike particle in the PT model, is subject to this field that is originated by the sample surface but modulated by the multiatomic nature of the particle contact layer.

This simplified picture of atomic friction at large contacts leads to the prediction of a number of superlubric states. The naive sinusoidal interaction (as felt by a single-atom apex) is recovered if the layer is rigid, albeit its amplitude is reduced depending on the layer size and its lattice mismatch with the surface potential. There exist several superlubric sizes for a given misfit ratio parameter, which minimize the effective potential amplitude. To design a nondissipative interface, one should consider such sizes.

Superlubricity can also be a result of other multiatomic properties of the apex layer. As a rule of thumb, we found that the kinetic friction becomes smaller as the atomic layer becomes longer or stiffer. Based on the inspection of details of the atomic configurations, we attribute this behavior to an increase of the number of intermediate short atomic slips when the chain becomes longer, while if the atoms are bound more strongly together a collective feature is enhanced: disappearing some of the independent atomic slips at the cost of synchronizing some other ones. Both effects suppress the discontinuity in the sliding motion and decrease the kinetic friction. In other words, increasing the number of degrees of freedom, and more collectively exciting them, the results of increasing N and κ, respectively, are two origins of friction reduction at the multiatomic interfaces.

The edge atoms, lacking at least one bonding, are less coordinated compared to the inner atoms. Therefore, they may refuse to contribute to the less-frictional collective motion on

the surface if the intra-layer coupling is weak. This way, the edge atoms play a critical role in increasing the friction on average as they get more easily stuck in the surface energy minima to lock the layer to the surface.

ACKNOWLEDGMENTS

Financial support by Iranian Science Elite Federation (Grant No. 11/66332) is acknowledged. The author greatly thanks two anonymous reviewers for their insightful comments and suggestions.

APPENDIX A: NUMERIC ALGORITHM

The equilibrium configuration of the atomic contact layer minimizes the effective potential energy, Eq. (7), for a given x_p. In practice, one implements a computer program that properly alters the atomic positions, collectively denoted by the vector $\mathbf{x} = (x_1, x_2, \ldots, x_N)^{\mathrm{T}}$, in the direction of descent of the energy. Even though nonquadratic terms contribute to v_{N}, the minimization can be done iteratively taking Newton steps $\mathbf{x} \leftarrow \mathbf{x} + \alpha\Delta\mathbf{x}$, where the positive parameter $\alpha < 1$ is tuned dynamically: α is increased (decreased) by, e.g., 5% upon energy decrement (increment) to speed up the convergence (prevent overjumping the well minimum). The step vector $\Delta\mathbf{x}$ solves the system of linear equations $\mathbf{k}\Delta\mathbf{x} = \mathbf{f}$. At each iteration, the Hessian matrix $\mathbf{k}$ and the force vector $\mathbf{f}$, given by Eq. (11), are evaluated from the chain configuration $\mathbf{x}$ at the previous iteration. If the iteration starts from an initial configuration that is not too far from the equilibrium, only after a few (typically two to five in case of $N < 10$) Newton iterations, $\|\mathbf{f}\|$ vanishes to within the machine precision, i.e., the configuration is relaxed. The reason is that the Hessian matrix $\mathbf{k}$ is positive definite in most points $\mathbf{x}$ of the configuration space. In addition, solving numerically the linear system of equations benefits highly from the symmetric tridiagonal structure of the Hessian matrix with a much lower computational cost. We employed the Thomas algorithm with $O(N)$ operations [31]. These two factors, give this static approach a considerable advantage over the dynamic approaches, which are computationally expensive; see Sec. V.

Figure 7 illustrates how the algorithm works where we consider a rigid cantilever ($\kappa_{\mathrm{dr}} \gg 1$) so that $x_p = x_s$. Once the particle takes a random step forward, the position of the well minimum on the energy landscape (shown by thin curves for successive support positions) advances, too. The apex catches the new well minimum in a few steps. It is seen that even if the well disappears and the apex needs to slip to the next well, the procedure works very efficiently by taking large steps in the beginning followed by shorter ones close to the well minimum. For demonstration purpose, here we assumed that the apex consists of a single atom ($N = 1$). For a multiatomic contact layer, a similar downhill skiing takes place on the N-dimensional hypersurface $v_N(x_p; \mathbf{x})$ per each particle position x_p. multiple slips and large jumps over several basins, observed in experiment [32], may happen if the steps of the support motion are not limited to very small ones (corresponding to high-speed support motion).

If the cantilever is elastic (finite κ_{dr}), after updating the apex configuration to achieve $f_i = 0$, the support position is also updated to $x_s = x_p + (x_p - x_a)/\kappa_{\mathrm{dr}}$ to nullify the net force on the particle body, Eq. (9). Note that when the suggested backward correction of the support position exceeds the initial trail forward step, the apex has experienced a slip and taken over the particle body, and thus the particle body would need to jump, too. In this case, instead of correcting the support position we relax for a second time the particle-body position according to $x_p = (x_a + \kappa_{\mathrm{dr}} x_s)/(1 + \kappa_{\mathrm{dr}})$ followed by rerelaxing the apex layer to nullify f_i. Finally by updating the support position f_p is also nullified and the complete equilibrium is attained. As discussed in Appendix B, one may exclude completely the updating of the support position at the absence of thermal fluctuations of the particle or when the particle is massive.

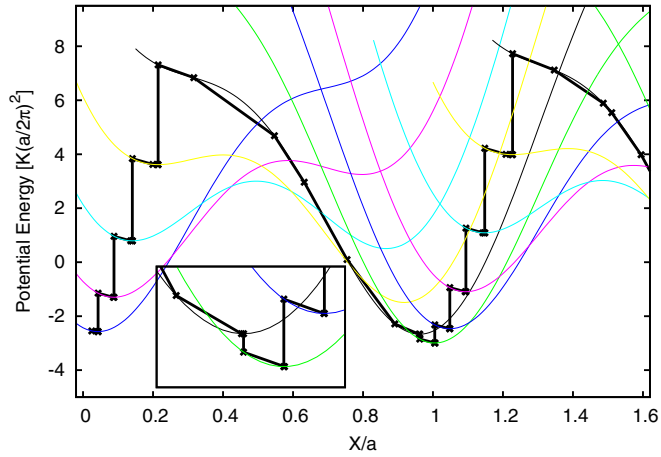

FIG. 7. Energy landscape of the PT particle, Eq. (14), with $\eta = 3$, and illustration of the energy minimization procedure. Each thin curve corresponds to one position of the support. The support advances stepwise by random steps not larger than $0.15a$, and the numeric algorithm suggests to the PT particle the positions shown by $\times$ symbols (and connected by the solid line to help the eye to track its path) to find iteratively the position with the minimum energy. Note: in the PT model the cantilever is rigid (the positions of the particle body and support are identical), so that the PT particle corresponds to the particle apex in our formalism.

APPENDIX B: NECESSITY OF INCLUDING THE LEVER ELASTICITY

As stated above, if the lever elasticity is not taken into account, the prolongation of the slip step at finite temperatures could not be explained. Here we show that at zero temperature, on the other hand, including the elasticity of the cantilever has no advantage but keeping the formalism unified.

In a numeric algorithm, such as the one addressed in Sec. III B, the procedure of relaxing the system when advancing the support consists of the following steps. First, a preliminary forward displacement is applied to the support (as the final step, a backward correction will refine this coarse displacement). x_p is then altered to laterally equilibrate the particle body between the apex and the support. However, then the apex atoms need to be brought back to equilibrium between the new position of the particle body and the sample surface. This rerelaxation of the apex configuration is done iteratively using

the multidimensional minimization procedure based on the Newton steps introduced in Appendix A. Again, the particle body needs to be equilibrated because its interaction with the apex has changed. In principle, alternating relaxation of x_p and $\mathbf{x}$ has to be done until self-consistency is achieved, i.e., $f_p = f_i = 0$ to within the desired accuracy. However, this expensive alternating relaxations may be avoided. The trick is that after the first relaxation of the apex and body, a correcting (backward) motion is applied to the support so that no rerelaxation of the apex is required because the particle body is not changed. To summarize, a fully equilibrated system is obtained by taking four steps: (i) support coarse displacement, (ii) particle body relaxation, (iii) apex layer relaxation, and (iv) support fine relaxation. It should be mentioned that the fine correction of the support position is accepted only if it does not lead to positioning the support behind its position at the previous step. This happens when the apex slips, which means that the particle body should also slip. In that case, such a support backward shift is waived, the second and third steps are done once more and only then a fine correction is applied to the support position.

Conceptually, the four-step procedure is equivalent to a two-step procedure where the support displacement is explicitly excluded. Starting from an already relaxed state, the particle body itself takes a step forward to a new position, and the apex configuration is then relaxed (iteratively). The instantaneous friction force is given by the second expression in Eq. (10) in terms of the relaxed particle-apex lateral separation $x_p - x_a$. If the cantilever is rigid, the particle body and the support coincide. For an elastic cantilever, however, one finds the corresponding support position as $x_s = x_p + \kappa_{\rm dr}^{-1}(x_p - x_a)$ by applying the condition $f_p = 0$ to Eq. (9). Interestingly, this leads to another expression for the friction force in terms of support-apex separation as $f_s = (1 + \kappa_{\rm dr}^{-1})^{-1}(x_s - x_a)$.

The latter resembles a single-spring PT model [see Eq. (16)] and implies that at zero temperature a two-spring model with spring constants $K_{\rm lever}$ and $K_{\rm apex}$ is identical to the basic PT model with a single-spring connecting the apex to the support and having a stiffness equivalent to that of the two springs in series, i.e., $1/(K_{\rm apex}^{-1} + K_{\rm lever}^{-1})$. The corresponding corrugation parameter reads

$$\eta = \left(1 + \kappa_{\rm dr}^{-1}\right)\frac{2\pi^2 E}{K a^2},$$

which differs from Eq. (3) by a larger-than-unit prefactor. We emphasize again that if the particle body is thermally activated, the cantilever comes back into play and plays a critical role [20,25]. Even at zero temperature, including the cantilever elasticity helped us to keep the formalism for a multiatomic apex layer identical to that of the basic PT model but with an effective potential v_N.

APPENDIX C: DYNAMIC VS STATIC SIMULATIONS

To evaluate the friction as a function of support position $f_s(x_s)$, first the equilibrium configuration of the particle body and its apex need to be determined. The solution $(x_p; \mathbf{x})$ to $f_p = \|\mathbf{f}\| = 0$ is not unique and the structure is equilibrated if trapped in any of the local minima of the potential energy landscape. Indeed, the system does not necessarily choose the ground state but its current state depends on its dynamics history. A reasonable approach to find the same tip trajectory as in experiment is to perform molecular dynamics (MD) simulations to integrate the Langevin equations of motion $m_i\ddot{x}_i = f_i - \gamma\dot{x}_i + \xi_i(t)$ for the N atoms, and also an additional one for the particle body if its effective mass is not too large. The drift forces $-\gamma\dot{x}_i$ simulate the energy dissipation while random forces $\xi_i(t)$ are responsible for pumping in the energy with a rate proportional to the temperature T. To realize this feature, the random forces are picked from a normal distribution satisfying the fluctuation-dissipation theorem, $\langle\xi_i(t)\rangle = 0$ and $\langle\xi_i(t)\xi_j(t')\rangle = 2\gamma k_B T\delta_{ij}\delta(t - t')$. Because the forces f_i depend on positions $x_p, x_i, x_{i\pm1}$, the $N + 1$ equations are coupled together and all are solved at each time step. Starting from an initial (equilibrium or randomized) configuration, the positions are updated in response to stepwise motions of the support. At each support position, after a sufficiently large number of time steps to ensure that the steady state is achieved, the MD simulation is still continued for collecting the data (in particular, friction) needed to calculate the time averages. The principal advantage of MD simulations is that temperature and support velocity explicitly come into the play. However, there are a number of drawbacks. For example, the results depend on the choice of effective mass of the particle body and atoms, effective damping parameter γ, and several other empirical quantities. In addition, the validity and robustness of MD simulations depends on the integration accuracy and the length of the time step. Conventional MD simulations may become soon computationally expensive for large systems if not only chain atoms but also sample atoms are explicitly treated.

An MD simulation is not the only way to determine the true configuration of the system. The system dynamics may be extracted also from its static properties (stable configurations and transition paths). This approach suits the present problem because the particle and its apex get stuck in basin minima for a while, while slipping very quickly over the barrier, meaning that only a small region of the configuration space is practically accessible by the system and thus relevant to its dynamics. In other words, the system trajectory in the configuration space is highly concentrated around only a few extrema of the $N + 1$-dimensional potential energy surface. Our static method concerns only this region of the configuration space. We move the support stepwise and essentially similar to an MD simulation. The particle position and its apex configuration are then optimized downhill into the minimum of the closet energy valley, as explained before. This way, the same trajectory as in a standard MD simulation is followed by the system and the procedure shares with MD simulation the required feature of being history aware. One notable advantage of the proposed procedure of repeated activation-relaxation is that the steps of the support displacement may be as long as a fraction of the lattice constant a, namely orders of magnitude larger than that in a real-time MD simulation. This reduces considerably the computational cost in particular for long chains or two-dimensional contacts. In addition, the procedure is free of MD empirical parameters, e.g., effective damping constants or mass.

APPENDIX D: IMPROVING EFFECTIVE POTENTIAL

For a nanoobject with an arbitrary configuration of the atoms at its apex layer all multiatomic-dependent properties including contact size, interatomic distances, and arrangement, bonding strength, etc. as well as thermal fluctuations of the apex all are encapsulated in the effective potential. Employing realistic model systems helps to improve the accuracy of the particle-sample interaction field. For example, density-functional theory calculations, performed on a number of representative particle positions and interpolated for intermediate positions, can provide a reliable effective potential where all atomic and electronic degrees of freedom of a few atomic layers of the sliding abject and the surface are accurately taken into account.

Note that several parameters affect the frictional behavior. We divide them into two families: structural properties and external parameters. The present study focuses on the structural properties, including the number of atoms (contact size), coupling strength and particle-substrate lattice mismatch. Studying the effect of external parameters, e.g., temperature and support velocity, which are kept practically zero in the present work, is a subject for future work. Here we give only an outlook of possible extension to the introduced procedure. In the simplest scenario, an effective potential, which is temperature-dependent in an average manner, can be constructed if the atomic positions are thermally randomized. Alternatively, the temperature can be applied directly using stochastic approaches. While the equilibrium configuration as a function of support position is determined by following the direction of the gradient of the effective potential (calculated at zero temperature), thermal noises are introduced via random displacements into the spatial degrees of freedom. A trail displacement is accepted either if the energy decreases or if the energy increment satisfies the condition given by the Metropolis algorithm.

[1] I. L. Singer and H. Pollock, *Fundamentals of Friction: Macroscopic and Microscopic Processes*, Vol. 220 (Springer Science & Business Media, Berlin, 2012).

[2] E. Gnecco, R. Bennewitz, T. Gyalog, C. Loppacher, M. Bammerlin, E. Meyer, and H.-J. Güntherodt, Velocity Dependence of Atomic Friction, Phys. Rev. Lett. **84**, 1172 (2000).

[3] P. Reimann and M. Evstigneev, Nonmonotonic Velocity Dependence of Atomic Friction, Phys. Rev. Lett. **93**, 230802 (2004).

[4] B. Bhushan, J. N. Israelachvili, and U. Landman, Nanotribology: Friction, wear and lubrication at the atomic scale, Nature (London) **374**, 607 (1995).

[5] M. Dienwiebel, G. S. Verhoeven, N. Pradeep, J. W. M. Frenken, J. A. Heimberg, and H. W. Zandbergen, Superlubricity of Graphite, Phys. Rev. Lett. **92**, 126101 (2004).

[6] A. Socoliuc, R. Bennewitz, E. Gnecco, and E. Meyer, Transition from Stick-Slip to Continuous Sliding in Atomic Friction: Entering a new Regime of Ultralow Friction, Phys. Rev. Lett. **92**, 134301 (2004).

[7] M. Hirano, Superlubricity: A state of vanishing friction, Wear **254**, 932 (2003).

[8] E. Cihan, S. Ipek, E. Durgun, and M. Z. Baykara, Structural lubricity under ambient conditions, Nature Commun. **7**, 12055 (2016).

[9] S. Kawai, A. Benassi, E. Gnecco, H. Söde, R. Pawlak, X. Feng, K. Müllen, D. Passerone, C. A. Pignedoli, P. Ruffieux *et al.*, Superlubricity of graphene nanoribbons on gold surfaces, Science **351**, 957 (2016).

[10] L. Wang, X. Zhou, T. Ma, D. Liu, L. Gao, X. Li, J. Zhang, Y. Hu, H. Wang, Y. Dai *et al.*, Superlubricity of a graphene/mos2 heterostructure: A combined experimental and dft study, Nanoscale **9**, 10846 (2017).

[11] C. H. Scholz, Earthquakes and friction laws, Nature (London) **391**, 37 (1998).

[12] P.-P. Cortet, M.-J. Dalbe, C. Guerra, C. Cohen, M. Ciccotti, S. Santucci, and L. Vanel, Intermittent stick-slip dynamics during the peeling of an adhesive tape from a roller, Phys. Rev. E **87**, 022601 (2013).

[13] C. M. Mate, G. M. McClelland, R. Erlandsson, and S. Chiang, Atomic-Scale Friction of a Tungsten Tip on a Graphite Surface, Phys. Rev. Lett. **59**, 1942 (1987).

[14] N. Varini, A. Vanossi, R. Guerra, D. Mandelli, R. Capozza, and E. Tosatti, Static friction scaling of physisorbed islands: The key is in the edge, Nanoscale **7**, 2093 (2015).

[15] A. Benassi, M. Ma, M. Urbakh, and A. Vanossi, The breakdown of superlubricity by driving-induced commensurate dislocations, Sci. Rep. **5**, 16134 (2015).

[16] M. Ma, A. Benassi, A. Vanossi, and M. Urbakh, Critical Length Limiting Superlow Friction, Phys. Rev. Lett. **114**, 055501 (2015).

[17] D. Dietzel, J. Brndiar, I. Štich, and A. Schirmeisen, Limitations of structural superlubricity: Chemical bonds versus contact size., ACS nano **11**, 7642 (2017).

[18] S. Cahangirov and S. Ciraci, Superlubricity in layered nanostructures, in *Fundamentals of Friction and Wear on the Nanoscale* (Springer, Berlin, 2015), pp. 463–487.

[19] S. Kawai, M. Koch, E. Gnecco, A. Sadeghi, R. Pawlak, T. Glatzel, J. Schwarz, S. Goedecker, S. Hecht, A. Baratoff *et al.*, Quantifying the atomic-level mechanics of single long physisorbed molecular chains, Proc. Nat. Acad. Sci. USA **111**, 3968 (2014).

[20] S. Maier, Y. Sang, T. Filleter, M. Grant, R. Bennewitz, E. Gnecco, and E. Meyer, Fluctuations and jump dynamics in atomic friction experiments, Phys. Rev. B **72**, 245418 (2005).

[21] P. Y. Le Daeron and S. Aubry, The metal-insulator transitions in the Peierls chain, J. Phys. C **16**, 4827 (1983).

[22] L. Prandtl, Ein gedankenmodell zur kinetischen theorie der festen körper, J. Appl. Math. Mech. **8**, 85 (1928).

[23] G. A. Tomlinson, A molecular theory of friction, Philos. Mag. J. Sci. **7**, 905 (1929).

[24] L. Jansen, H. Hölscher, H. Fuchs, and A. Schirmeisen, Temperature Dependence of Atomic-Scale Stick-Slip Friction, Phys. Rev. Lett. **104**, 256101 (2010).

[25] D. G. Abel, S. Yu. Krylov, and J. W. M. Frenken, Evidence for Contact Delocalization in Atomic Scale Friction, Phys. Rev. Lett. **99**, 166102 (2007).

[26] T. Kontorova and J. Frenkel, On the theory of plastic deformation and twinning, Zh. Eksp. Teor. Fiz. **8**, 1340 (1938).

[27] O. M. Braun and Y. Kivshar, *The Frenkel-Kontorova Model: Concepts, Methods, and Applications* (Springer Science & Business Media, Berlin, 2013).

[28] T. Zanca, F. Pellegrini, G. E. Santoro, and E. Tosatti, Frictional lubricity enhanced by quantum mechanics, Proc. Nat. Acad. Sci. USA **115**, 3547 (2018).

[29] M. Weiss and F.-J. Elmer, Dry friction in the frenkel-kontorova-tomlinson model: Static properties, Phys. Rev. B **53**, 7539 (1996).

[30] M. Weiss and F.-J. Elmer, Dry friction in the frenkel-kontorova-tomlinson model: Dynamical properties, Z. Phys. B **104**, 55 (1997).

[31] L. H. Thomas, Elliptic problems in linear difference equations over a network, Watson Scientific Computing Laboratory Report, Columbia University, New York, 1949.

[32] S. N. Medyanik, W. K. Liu, I.-H. Sung, and R. W. Carpick, Predictions and Observations of Multiple Slip Modes in Atomic-Scale Friction, Phys. Rev. Lett. **97**, 136106 (2006).